**Contract No.:**

This manuscript has been authored by Battelle Savannah River Alliance (BSRA), LLC under Contract No. 89303321CEM000080 with the U.S. Department of Energy (DOE) Office of Environmental Management (EM).

# Preventing Tritium Memory Effects in Ion Chambers Using Ultraviolet LEDs

George K. Larsen[1], Khai Nguyen[1], and Simona E. Hunyadi Murph[1,2]

[1]*Savannah River National Laboratory, Aiken, SC 29808 USA*
[2]*University of Georgia, Athens, GA 30602 USA*

*Abstract*— Ion chambers are often employed to measure the concentration of tritium within flowing gases. In real world environments the active surfaces of ion chambers become covered with tritiated surface contaminants. This tritiated surface contamination often creates a large background response that can mask the signature of interest, which is the tritium concentration in the gas phase. Previous efforts to reduce the effects of surface contamination in ion chambers utilize inert coatings (e.g., gold) and low surface area electrodes (e.g., wire mesh). These strategies only reduce the effect and do not provide information regarding the ratio of the current from the contaminated surface to the current from the volume of the detector. Additionally, gold coating is expensive, substantially increasing the cost of the instrument. While ion chambers may be periodically cleaned, this recurring hands-on task does not adequately address tritium level ambiguities in gloveboxes and increases the risk of detector damage and worker exposure. An ideal solution to this issue would be to either develop an ion chamber that does not accrue surface contamination, or one that is self-cleaning while it is in operation. In this report we describe the development of using ultraviolet (UV) LED light illumination to desorb contamination from ion chambers while they are in operation, preventing the negative effects of surface contamination.

*Index Terms*— Decontamination, ion chambers, UV light, radiation detectors, tritium.

## 1. Introduction

Radiation detectors often suffer from “memory effects” upon repetitive uses in industrial settings. Memory effects means that the radioactive material may interact in some way with, and be retained by, the detector. The detector may respond to radioactive material that is retained on the detector, thus providing a response even though the air currently being monitored contains no radioactive materials. As a result, the detector "remembers" the radiation response measured in the previous air measurement [1]. While any radiation detector may experience memory effects due to surface contamination, the following detectors are most prone to experience such effects: (1) Gaseous ionization detectors (ion chambers, proportional counters, Geiger counters) [2, 3]; (2) Scintillation detectors, both organic and inorganic [4, 5]; and (3) Beta induced X-ray spectrometry (BIXS) [6]. Non-radioactive surface contamination from water and absorbed species can also negatively affect radiation detectors. For example, stray current can leak across the surfaces of insulators that are covered with non-radioactive contamination, leading to higher background signals in gaseous ionization detectors [7]. Thus, there is a need of improving the performance of radiation detectors by eliminating or reducing memory effects through removal of both non-radioactive and radioactive contamination from detector surfaces while in operation.

Ion chambers are often employed to measure the concentration of tritium within flowing gases and glovebox atmospheres. The basic concept is straightforward: tritium decay ionizes background gas molecules, and these ionized molecules produce a current within an applied electric field. This ionic current is measured providing an electrical readout of the tritium concentration. However, during operation, the active surfaces of ion chambers may become covered with surface contamination that can retain tritium. This tritiated surface contamination will contribute to the measured current of the ion chamber, creating a large background response that can obscure measurement of the actual tritium concentration in the gas phase. This memory effect is especially problematic for the detection of tritium due to the isotopic exchange between tritium in the volume with surface species that contain hydrogen (protons or deuterons).

Previous efforts to reduce the effects of surface contamination in ion chambers utilize low surface area electrodes (*e.g.*, wire mesh) [8], but this route only reduces the effect and does not necessarily provides accurate information regarding the ratio of the current from the contaminated surface to the current from the volume of the detector. That is, ambiguity between signals from the surface species and the gas phase species will remain, especially in dynamic systems. Alternatively, ion chambers may be periodically cleaned. However, periodic cleaning does not address tritium level ambiguities in gloveboxes and increases the risk of detector damage and worker exposure. An ideal solution to this issue would be to either develop an ion chamber that does not accrue surface contamination, or one that is self-cleaning while it is in operation.

In this report we investigate ultraviolet (UV) LED light illumination to desorb contamination from ion chambers while they are in operation, preventing the appearance of the negative effects of surface contamination. The concept is based on studies showing that UV light illumination can been used to remove surface contamination and create atomically clean metal surfaces for devices.[9, 10] The concept also benefits from the rapid improvement in LED technology over the past several years that affords low cost, robust, long-lasting, and powerful light sources that can stimulate desorption.

## 2. Proof-of-Concept Testing

### *2.1. Experimental Methods*

Initial testing of in situ photo-cleaning employed an existing gold coated “bird cage” style of ion chamber and an ion chamber calibration manifold. The calibration manifold includes a quartz window for illuminating the ion chamber externally from the side (**Fig. 1**). Additionally, a test stand was assembled to support the vessel that contains the ion chamber and to hold a spot curing UV LED system (ThorLabs). The LED central wavelength is $\lambda$ = 365 nm, which outputs a maximum power of 135 mW/cm$^2$ at the focus. However, the power delivered in this setup is significantly less since the ion chamber is placed at large distance from the focus in order to obtain an even spread of light illumination across its surface as possible. UV illumination of the lower insulators can be seen in Fig 1c, showing the beam’s divergence. It is also important to note that a single LED illuminating from the side is not expected to be optimal for decontamination but is sufficient to demonstrate the proof-of-concept.

The basic test procedure consists of exposing the manifold to trace levels of tritium within a nitrogen background at 1 atm for thirty minutes. Afterward, the tritium source is closed, and the manifold is purged. The purge gas consists of atmospheric air at 1 atm that is pulled in by a vacuum

pump from the laboratory. A rotameter was used to set a flowrate of 10 CFH (~4.7 lpm). The exposure conditions are listed in the Appendix. The manifold contains both a reference ion chamber and a birdcage ion chamber. The reference ion chamber has a volume of 0.99 L, and the birdcage ion chamber has a volume of 3.2 L. The background current for these ion chambers prior to tritium exposure is typically around $10^{-14}$ A and is limited by leakage current.

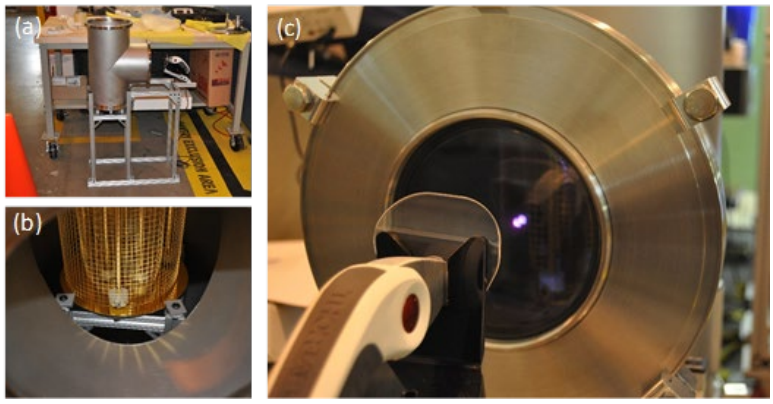


***Fig. 1.*** *Photographs of the ion chamber test stand: (a) the tee-shaped vessel and the handheld UV system mounts; (b) the gold coated ion chamber inside test vessel; and (c) the ion chamber under UV LED illumination*

The birdcage ion chamber is either left in the dark or illuminated by the UV LED as shown in **Fig. 1** for dark and UV experiments, respectively. The UV light is turned on at the beginning of the purge, as described in Table I in the Appendix, and turned off at the completion of each test. The reference ion chamber is based on a spherical design and remains in the dark for all experiments. It is important to note that ion chamber structure (e.g., "bird cage" versus spherical) plays a large role in its response [11]. However, the reference ion chamber provides an additional control that can account for experimental variability. Due to the experimental process and setup, "Dark" experiments must be run on separate days than "UV" experiments. The ambient conditions typically change daily, and therefore, the comparison against the reference for the both the "Dark" and "UV" experiments allows for control against these variations. These conditions are representative of 'real' environments and experimental settings. The radiation induced currents for both ion chambers are monitored during the purge procedure by a picoammeter (Keithley 6517B). The relatively low level of light illumination used in the UV experiments did not induce a noticeable response in the picoammeter.

Eleven tests were conducted in which the ion chamber was exposed to tritium and subsequently purged. Tests 1 – 4 involved preliminary scoping experiments to test the procedure and manifold. Test 5 and beyond were designed for data collection, and the results are discussed below. The test run labels are based on internal usage, showing the sequencing of the tests. The experimental variation between these tests is due to the variability of the ambient conditions occurring on different days. These conditions can be found in the Appendix. Finally, it is worthwhile to note that the observed operational range in these experimental runs is set by the amount of surface contamination that is built up by exposure to tritiated gas, which is determined by the initial activity within the monitor, the duration of the exposure and the detector temperature. In these cases, surface contamination did not exceed greater than two decades above background.

*2.2. Results and Discussion*

The results of the experiments are presented in **Fig. 2**, which plots the ion chamber (IC) current versus time during the purge procedure for both the UV and dark experiments. The overall magnitude and change in the IC current versus time depends on a number of variables including temperature, humidity, previous history, and minor adjustments at the start of each test (see Table in the Appendix). Thus, there are experimental variations which contribute to IC current magnitude and how quickly it approaches background in addition to that of UV LED illumination. However, the UV illuminated purges exhibit a noticeably faster recovery to baseline, except for Test 6, which may have been affected by a buildup of contamination from the previous five dark experiments. Test 6 may appear as an outlier at first glance, but this is because this run is expected to have the highest level of initial surface contamination of these experiments. Thus, the higher IC current measured is likely the result of more tritium outgassing from the surfaces. Similar behavior has been observed in the UV removal of water from surfaces during vacuum pumping [12].

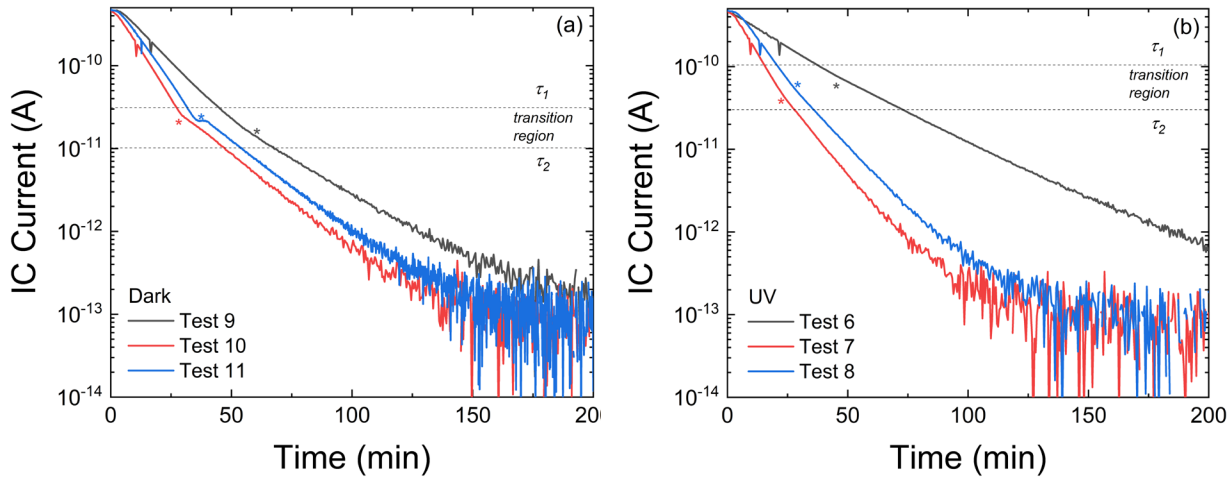


***Fig. 2.*** *Ion chamber (IC) current versus time during the purging experiments (a) under UV LED illumination and (b) in the dark. The asterisks denote the apparent inflection point in behavior.*

In all of the plots, the change in the IC current appears to have two different regions: an initial decay region and a second decay region, with a slightly variable transition between them. We postulate that the tritium in the gas phase dominates the signal in the initial decay region as tritium is purged and physiosorbed tritium is desorbed from surfaces throughout the manifold, including the ion chamber. The tritium contamination on the ion chamber surface will have a larger effect in the second decay region. For the dark experiments, the decay in the second region is notably much slower, which is also observed by a characteristic inflection point, or kink, in the plots. This feature is clearly observed in all of the dark experiments, but only subtly in the UV experiments. It is also observed in dark tests that preceded the UV experiment (**Fig. 3**), and thus, is specific to the dark experiments and not the UV.

The behavior seen in the IC current during these experiments is similar to ion chamber current signals collected during tritium glovebox stripping experiments described by Klein and Wermer [13]. They observed a sharp inflection after the initial tritium stripping activity was completed and

the glove box activity became governed by the rate of outgassing of components. Further, they found that the glovebox tritium concentration initially decreased rapidly but began to plateau or "hang," which they hypothesized occurred when the tritium sequestration rate became roughly equal to the tritium outgassing rate. In the experiments presented here, fresh air is continuously pulled in and the effluent is vented to stack, and therefore, it can be assumed that the rate limitations after the inflection point is driven primarily by tritium outgassing. Thus, by separately analyzing the dynamics of the two regions, before and after the inflection point, one can obtain direct comparison for the cases when (1) the ion chamber current is primarily determined by the manifold purge rate and (2) the ion chamber current is determined by the outgassing rate.

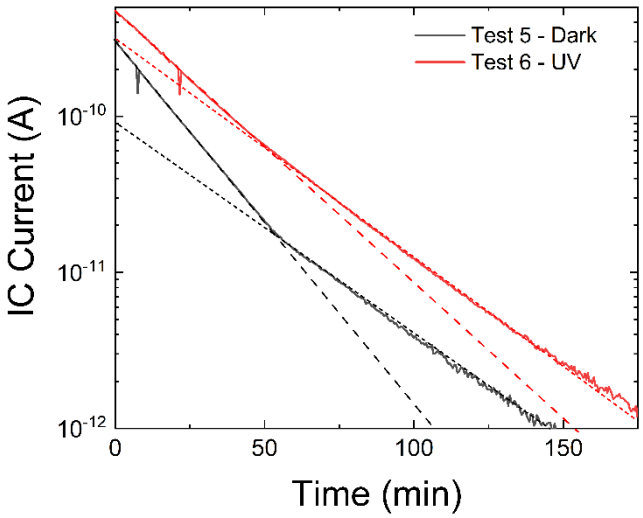


***Fig. 3.*** *IC current versus time during the purging experiments showing the distinctive inflection point for representative dark and UV experiments. The dashed and dotted lines are guides for the eye to help visualize the inflection points.*

In order to quantitatively compare the results from the experiments, the different data sets were fit to an exponential decay equation.: $I(t) = A\ \mathrm{Exp}[-t/\tau_n] + I_0$, where $\tau_n$ is the corresponding decay constant, $A$ is a constant related to the initial current, and $I_0$ corresponds with the baseline current. The Reference IC current was fit to a single exponential decay with $\tau_{ref}$ as the decay constant. The birdcage IC current was fit to two different exponential decays, one covering the first region and the other covering the second, lower current region. The exponential time constants for these two different regions are $\tau_1$ and $\tau_2$, respectively. The fitting results are presented in the **Table I** in the Appendix.

The experimental variation between each run can be minimized by comparing the different time constants within each test run. **Fig. 4a** plots $\tau_2/\tau_1$ and demonstrates that the time constants $\tau_1$ and $\tau_2$ are more similar for the UV tests than for the dark tests. This can be seen by visual inspection of **Fig. 3** where there is a noticeable transition for the dark and not UV. **Fig. 4b** compares $\tau_1/\tau_{ref}$ and shows that the initial decay region is generally faster for the UV tests and improves with increasing UV exposure. Note that Test 6 had a 700s delay before the UV light was turned on. The dark experiments fluctuate around the same value. **Fig. 4c** compares $\tau_2/\tau_{ref}$ and demonstrates that the second decay region, when normalized by $\tau_{ref}$, is always faster for the UV tests. Again, the dark

experiments fluctuate around the same value, while improvement is observed for increasing UV exposure cycles. The second decay region is expected to be more sensitive to surface contamination of the IC. Ultimately, the results show that UV LED illumination appears to change the dynamics of Region 2 such that they are similar to Region 1, which suggests that the rate limiting step becomes purge related, and not outgassing related, for both regions. It is also worth noting that the transition between Regions 1 and 2 also occurs at higher IC currents, which is consistent with increased outgassing throughout and is similar to behavior seen in UV assisted desorption for vacuum pumping [12].

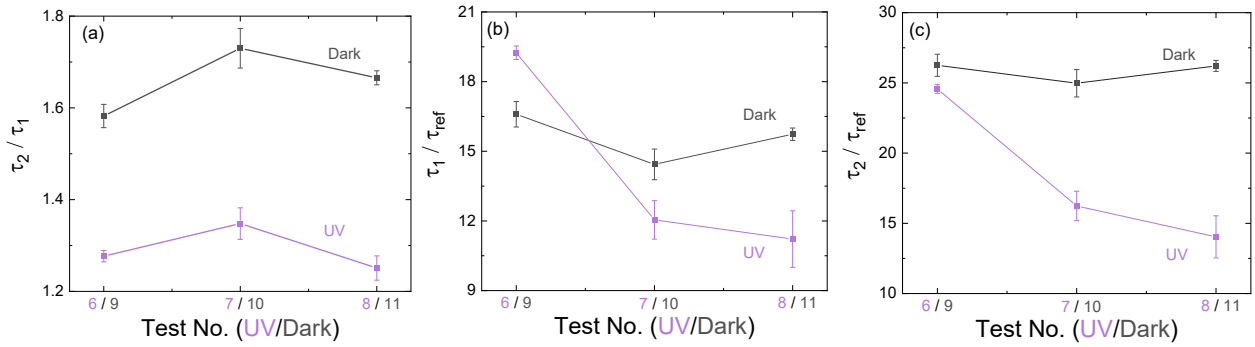


***Fig. 4.*** *Comparisons between the different decay constants for the different tests: (a) plots the second decay region normalized by the first decay region, $\tau_2/\tau_1$, for each run; (b) plots the first region normalized by the reference IC, $\tau_1/\tau_{ref}$, for each run; (c) plots the second decay region normalized by the reference IC, $\tau_2/\tau_{ref}$, for each run. The error bars in the figure reflect the statistical error from the curve fits.*

The results described above are promising and show that a single UV LED mounted on the outside of a test assembly can stimulate faster "memory" recovery and a lower baseline for a bird cage ion chamber. The observed effects are attributed to the photo-effects of UV illumination, as the relatively low level of illumination does not generate any appreciable thermal effects. Such photo-effects may include photocatalytic isotope exchange or photo-stimulated desorption. Elucidating the primary mechanisms observed here is part of ongoing research. Regardless of the mechanism, these results establish the proof-of-concept of a photo-cleaned ion chamber.

## 3. Prototype LED-integrated Ion chamber

### *3.1 Construction*

The promising results described in Section 2 were followed by the construction and assembly of prototype ion chambers with integrated LEDs that can enable in situ photo-decontamination of the surface. The design of the ion chambers is based on the original bird cage design illustrated above. However, one notable change is that the ion chambers will use uncoated stainless-steel surfaces instead of gold coated ones. Gold coating adds a significant cost to the ion chamber construction, and demonstrating the ability to photo-clean stainless-steel ion chambers using LEDs would represent a large cost savings by reducing the reliance on gold coatings to achieve low backgrounds and reduce the memory effect of surface contamination.

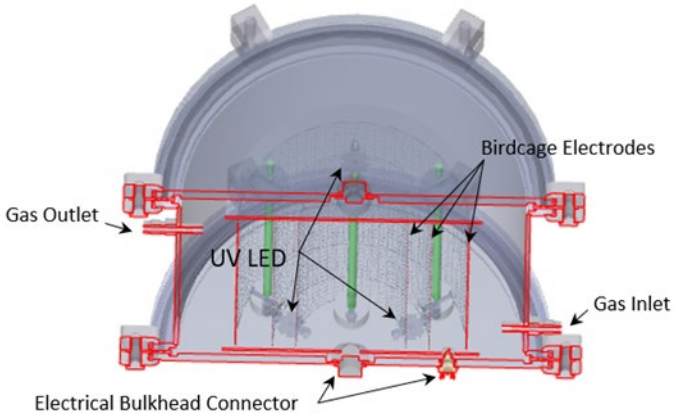


***Fig. 5.*** *CAD cross-section of ion chamber inside testing vessel.*

The ion chamber design was modified to accept LED light integration. In this case, 6 LEDs with center wavelengths of 365 nm are mounted on the outer plates of the ion chambers. Each plate holds three LEDs in place at 120° intervals, with the opposing plate offset by 60° to ensure uniform coverage on the electrode mesh (**Fig. 5**). Each LED is capable of outputs of 810 mW at a minimum with a viewing angle of 130°. A final prototype assembly is shown in **Fig. 6**

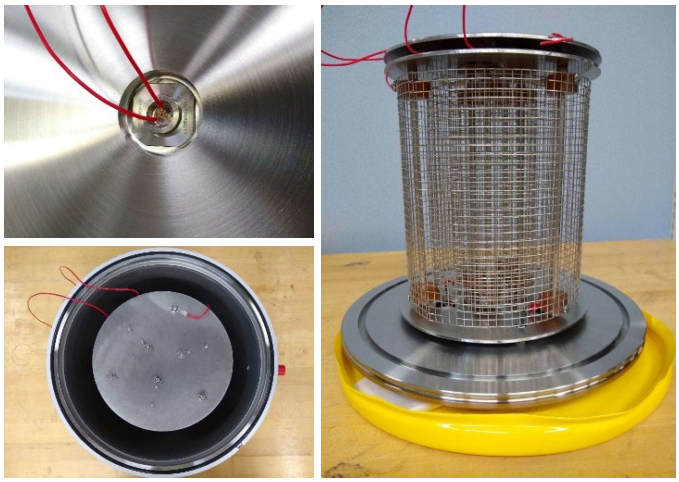

***Fig. 6.*** *Photographs of the prototype LED integrated ion chamber during assembly and at completion*

*3.2 Tritium Testing*

The tritium testing of the prototype followed the same test procedure used for the proof-of-concept, described in Section 2 above. The basic procedure involves exposing the ion chamber to a recirculating tritium/nitrogen gas mixture, followed by purging using room air pulled through a vacuum pump at a rate of 10 CFH (~4.7 lpm) and out the stack to create constant air flow while maintaining pressure slightly below ambient. Seven purging tests were performed. The first purge (Test I) was done under UV illumination, followed by three dark tests (Tests II - IV) and three UV

tests (Test V – VII). Background measurements were also taken with UV LEDs both on and off to observe any effects on the steady-state current of the ion chamber, and none were observed.
The data for Tests I - VII are presented in **Fig. 7**. The results are similar to those of the proof-of-concept testing. The dark experiments have similar or increasing background currents for increasing test cycles. In comparison, each UV exposure cycle reduces the background current, eventually to where the background disappears. Additionally, the initial UV experiments reach background faster than the dark experiments, and the UV experiments also achieve a lower base current than the dark experiments. A notable difference between these experiments and the proof-of-concept experiments (gold coated) is that these demonstrate the effectiveness of UV LED light for the in-situ decontamination of stainless-steel surfaces.

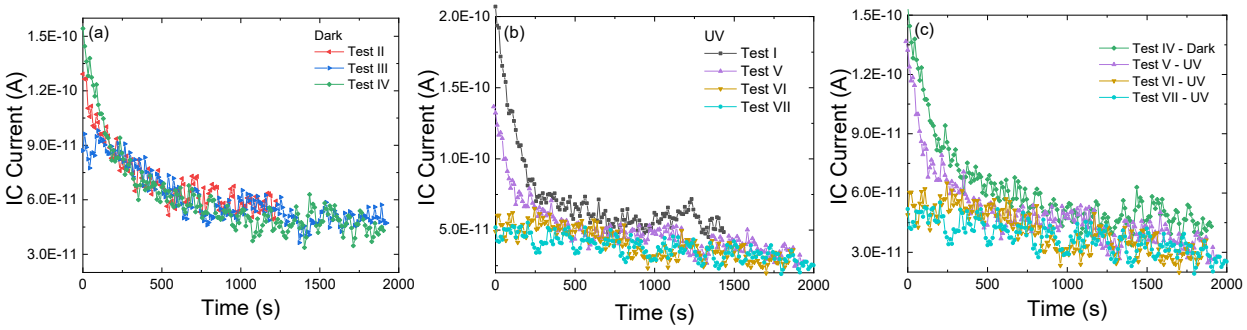


***Fig. 7.*** *Plot of ion chamber current versus time during purging experiments for the (a) dark and (b) UV LED experiments. (c) Direct comparison between selected dark and UV experiments*

## 4. Conclusions

This report describes the successful development of the concept of LED-cleaned backgroundless ion chambers. The construction and tritium testing of a working prototype demonstrated that UV LED integration can be used to promote in situ decontamination of a stainless-steel ion chamber while in operation. The results showed stainless steel surfaces illuminated by UV LEDs are decontaminated faster than non-illuminated stainless-steel surfaces. It was also demonstrated that the light illumination reduced the accumulation of ion chamber background signal after exposure to tritium. Thus, the LED integrated system functions as a backgroundless ion chamber. This is the first reported demonstration of this technology concept.

In addition to the many benefits of a backgroundless ion chamber, these results are also notable because it represents a large potential cost saving by negating the need for gold coatings, and it also suggests that LEDs can be employed to facilitate the detritiation of other stainless-steel surfaces and other radiation detector concepts. Finally, it is worthwhile to note that ion chambers with low surface areas and gold coatings may be decontaminated very rapidly [14]. However, the LED approach described here is advantageous when gold coatings are cost prohibitive and in cases where dry air purging is not feasible. Even in cases where purging is possible, our results demonstrate that UV LED illumination prevents background build-up and increases the rate of decontamination while purging, and therefore, can reduce both the number of occurrences and the time a detector must be taken offline.

**Acknowledgement**

The authors gratefully acknowledge Allen Quackenbush for the drawings and Blake Busby for designing and assembling the stand. The authors also acknowledge Mark Farrar, Joel Ingold, Tyler Guin, and Paul Foster for their valuable assistance with this project. This work was produced by Battelle Savannah River Alliance, LLC under Contract No. 89303321CEM000080 with the U.S. Department of Energy. Publisher acknowledges the U.S. Government license to provide public access under the DOE Public Access Plan (http://energy.gov/downloads/doe-public-access-plan). Financial support for this work was provided by the SRS Plant Directed Research, Development and Demonstration program

**References**

[1] R. Traub and G. Jensen, "Tritium radioluminescent devices, Health and Safety Manual," Pacific Northwest Lab., Richland, WA (United States)1995.

[2] M. Nishikawa, T. Takeishi, Y. Matsumoto, and I. Kumabe, "Ionization chamber system to eliminate the memory effect of tritium," *Nuclear Instruments and Methods in Physics Research Section A: Accelerators, Spectrometers, Detectors and Associated Equipment,* vol. 278, pp. 525-531, 1989/06/01/ 1989.

[3] K. Shank and C. Easterly, "Tritium instrumentation for a fusion reactor power plant," Oak Ridge National Lab.1976.

[4] C. E. Seifert, J. I. McIntyre, K. C. Antolick, A. J. Carman, M. W. Cooper, J. C. Hayes*, et al.*, "Mitigation of memory effects in beta scintillation cells for radioactive gas detection," *Proceedings of the 27th Seismic Research Review: Ground-Based Nuclear Explosion Monitoring Technologies,* pp. 804-814, 2005.

[5] S. Sheen, "NRC Job Code V6060: Extended in-situ and real time monitoring. Task 4: Detection and monitoring of leaks at nuclear power plants external to structures," Argonne National Lab.(ANL), Argonne, IL (United States)2012.

[6] M. Röllig, F. Priester, M. Babutzka, J. Bonn, B. Bornschein, G. Drexlin*, et al.*, "Activity monitoring of a gaseous tritium source by beta induced X-ray spectrometry," *Fusion Engineering and Design,* vol. 88, pp. 1263-1266, 2013/10/01/ 2013.

[7] G. F. Knoll, *Radiation detection and measurement*: John Wiley & Sons, 2010.

[8] L. Worth, R. Pearce, J. Bruce, J. Banks, and S. Scales, "Development of a novel contamination resistant ion chamber for process tritium measurement and use in the JET first trace tritium experiment," *Fusion science and technology,* vol. 48, pp. 370-373, 2005.

[9] J. R. Vig, "UV/ozone cleaning of surfaces," *Journal of Vacuum Science & Technology A,* vol. 3, pp. 1027-1034, 1985.

[10] B. D. Zion and S. J. Sibener, "UV Photodesorption of Novel Molecular Beam Induced NO Layers on NiO(111)/Ni(111)," *The Journal of Physical Chemistry C,* vol. 112, pp. 5961-5965, 2008/04/01 2008.

[11] Z. Chen, S. Peng, S. Cheng, Y. Li, and Y. Yang, "CFD calculations of response time for ionization chambers in tritium measurements," *Fusion Engineering and Design,* vol. 143, pp. 196-200, 2019/06/01/ 2019.

[12] S. R. Koebley, R. A. Outlaw, and R. R. Dellwo, "Degassing a vacuum system with in-situ UV radiation," *Journal of Vacuum Science & Technology A,* vol. 30, p. 060601, 2012.

[13] J. E. Klein and J. R. Wermer, "Tritium Stripping in a Nitrogen Glove Box Using Palladium/Zeolite and SAES ST 198," *Fusion Technology,* vol. 28, pp. 1532-1539, 1995/10/01 1995.

[14] Z. Chen, S. Peng, P. Chen, R. Chang, G. Wu, and Y. Li, "Improvement of ionization chamber for tritium measurements in in-pile tritium extraction experiments," *Fusion Engineering and Design,* vol. 147, p. 111222, 2019/10/01/ 2019.

## Appendix

***Table I***

*Experimental conditions and decay constants obtained through fitting for Proof-of-concept testing*

| Test | LED Status | Humidity (%) | $\tau_{ref}$ ($min^{-1}$) | $\tau_1$ ($min^{-1}$) | $\tau_2$ ($min^{-1}$) | $\tau_2 / \tau_1$ | $\tau_1 / \tau_{ref}$ | $\tau_2 / \tau_{ref}$ |
|---|---|---|---|---|---|---|---|---|
| **6** | On, $t$ = 700s | 46.1 | 1.21 ± 0.01 | 23.4 ± 0.2 | 29.9 ± 0.1 | 1.28 ± 0.01 | 19.2 ± 0.3 | 24.6 ± 0.3 |
| **7** | On, $t$ = 0s | 52.3 | 0.73 ± 0.05 | 8.8 ± 0.2 | 11.9 ± 0.1 | 1.35 ± 0.03 | 12.0 ± 0.8 | 16 ± 1 |
| **8** | On, $t$ = 0s | 55.5 | 1.0 ± 0.1 | 11.1 ± 0.2 | 13.9 ± 0.1 | 1.25 ± 0.03 | 11 ± 0.01 | 14 ± 1 |
| **9** | Off | 57.5 | 0.89 ± 0.03 | 14.6 ± 0.2 | 23.1 ± 0.1 | 1.58 ± 0.03 | 16.6 ± 0.5 | 26.2 ± 0.8 |
| **10** | Off | 55.2 | 0.72 ± 0.03 | 10.4 ± 0.3 | 18.1 ± 0.1 | 1.73 ± 0.04 | 14.4 ± 0.7 | 25 ± 1 |
| **11** | Off | 52.2 | 0.72 ± 0.01 | 11.3 ± 0.1 | 18.9 ± 0.1 | 1.67 ± 0.02 | 15.7 ± 0.3 | 26.2 ± 0.4 |

***Table II***

*Proof-Of-Concept Ion Chamber (3.2L) Radiation Measurement Data*

| Test | Background (A) | Tritium Exposure ($mCi/m^3$) | Temperature (°C) | Initial Current* (A) | Ending Current (A) |
|---|---|---|---|---|---|
| **5** | 2.95E-13 | 518 | 26.65 | 2.95E-10 | 4.67E-14 |
| **6** | 1.01E-13 | 516 | 25.67 | 4.57E-10 | 1.10E-13 |
| **7** | 9.45E-14 | 516 | 25.91 | 4.74E-10 | 1.88E-14 |
| **8** | 7.37E-14 | 515 | 25.40 | 4.74E-10 | 1.54E-14 |
| **9** | 6.29E-14 | 513 | 24.22 | 4.74E-10 | 5.28E-14 |
| **10** | 6.02E-14 | 512 | 24.09 | 4.69E-10 | 2.37E-14 |
| **11** | 6.49E-14 | 510 | 22.67 | 4.80E-10 | 1.29E-14 |

**Note the ion chamber currents reported in the table and throughout are values during purging. Therefore, the initial current measurement is related to the tritium activity, in both the atmosphere and in surface contamination, some time after the ion chamber was exposed to the tritium load/exposure conditions listed in the table.*

***Table III***

*LED-Integrated Ion Chamber (3.2L) Radiation Measurement Data*

| **Test** | **Background** (A) | **Tritium Exposure** ($mCi/m^3$) | **Temperature** (°C) | **Initial Current*** (A) | **Ending Current** (A) |
|---|---|---|---|---|---|
| **I** | 1.26E-11 | 472 | 20.75 | 1.94E-10 | 4.86E-11 |
| **II** | 1.54E-11 | 471 | 20.57 | 1.27E-10 | 5.93E-11 |
| **III** | 9.48E-12 | 469 | 19.29 | 9.62E-11 | 4.72E-11 |
| **IV** | 4.48E-12 | 469 | 19.37 | 1.45E-10 | 4.31E-11 |
| **V** | 1.22E-11 | 470 | 19.50 | 1.32E-10 | 2.76E-11 |
| **VI** | 2.15E-11 | 470 | 19.59 | 6.02E-11 | 3.61E-11 |
| **VII** | 9.87E-12 | 470 | 19.66 | 4.25E-11 | 2.53E-11 |

**Note the ion chamber currents reported in the table and throughout are values during purging. Therefore, the initial current measurement is related to the tritium activity, in both the atmosphere and in surface contamination, some time after the ion chamber was exposed to the tritium load/exposure conditions listed in the table.*